INTERNAL REPORT

Configuration study for a low-frequency aperture array at the SRT site

M. Murgia, F. Govoni, J. Monari, F. Perini,
and additional 23 co-authors.

Report N. 32, released: 24 Jan 2014

Reviewer: A. Possenti

OAC Osservatorio Astronomico di Cagliari

Configuration study for a low-frequency aperture array at the SRT site

M. Murgia[1], F. Govoni[1], J. Monari[2], F. Perini[2], Bianchi[2], P. Bolli[4], G. Comoretto[4], D. Dallacasa[3], F. Gaudiomonte[2], L. Gregorini[3], K.-H. Mack[2], F. Mantovani[2], M. Massardi[2], A. Mattana[2], A. Melis[1], L. Mureddu[1], G. Naldi[2], A. Poddighe[1], I. Porceddu[1], I. Prandoni[2], G. Pupillo[2], M. Schiaffino[2], F. Schillirò[2], G. Serra[1], T. Venturi[2], G. Virone[5], and A. Zanichelli[2].

([1]) INAF- Osservatorio Astronomico di Cagliari

([2]) INAF- Istituto di Radioastronomia di Bologna

([3]) Dipartimento di Fisica e Astronomia, Università di Bologna

([4]) INAF- Osservatorio Astrofisico di Arcetri

([5]) CNR IEIIT Torino

January 23, 2014

1 Abstract

We present the study of possible configurations for an aperture array constituted by prototypical low-frequency antennas designed to operate in the range 70 - 450 MHz. We focus on an array composed by a core plus a few satellite phased array stations to be installed to within the area of the Sardinia Radio Telescope (SRT) site. The purpose of this investigation is to verify the performances in terms of both uv-coverage and synthesized resolution resulting from different configurations of the array.

2 Introduction

This investigation is conducted in the context of a project[1] aimed to the study of new technologies for the observation of the sky at low radio frequencies. The goal of the project is the installation at the SRT site of an aperture array constituted by prototypical low-frequency antennas designed to operate in the range 70 - 450 MHz (hereafter Sardinia Aperture Array Demonstrator or SAD). As a first step, the project foresees a preliminary analysis aimed to determine which is the optimal composition of the array in terms of number and disposition of the antenna elements. Here we study an aperture array composed by a core plus a few satellite stations made by a large number of small, fixed antenna elements plus receiver chains which can be arranged in a regular or random pattern on the ground. A beam could be formed at station level and steered by combining all the received signals after appropriate time delays for phase alignment have been applied. In addition, it is possible to form a small number of relatively long baselines (a hundreds of meters in our case) between the phased array stations thus improving significantly the angular resolution of the aperture array by using the so-called Earth rotation synthesis technique.

The configuration of the stations is clearly constrained by the effective space which is available for the antenna installation at the site. Among all the possible array configurations that require similar installation efforts, we look for those that provide the most useful performances in terms of uv-coverage and angular resolution. Indeed, good uv-coverage and resolution are necessary for a scientific validation of the array based on the observation of astronomical radio sources.

3 The SRT site

The SRT site is located close the town of San Basilio, approximately 35 km north of the city of Cagliari. The area is a small plateau, locally known as "Pranu Sanguni", at an altitude of about 600 m above the sea level and that is surrounded by hills range from 500 to 700 m in height. The geographical coordinates are Latitude 39d 29m 34s N and Longitude 9d 14m 42s E (see Fig. 1). The actual site perimeter is outlined by a red line in the right panel of Fig. 1. However, the fencing of this perimeter is currently under revision, thus it is important to reach conclusive results about the array configuration as soon as possible. The actual site area span about 530 m in north-south direction and about 300 m in east-west direction.

[1]L.R. 7 Agosto 2007, N.7 : "Promozione della Ricerca Scientifica e dell'innovazione Tecnologica in Sardegna", Progetti di ricerca fondamentale o di base annualità 2012; CRP-60151, PI M.Murgia.

The SRT 64 m single-dish antenna occupies the northern side of the site while the observatory buildings are aligned to the Eastern border. The remaining part of the site landscape is characterized by a rough terrain with a relatively flat relief (see inset of Fig. 1). Preliminary low-frequency RFI investigations at the site has been conducted by Govoni et al. (2013) and Murgia et al. (2013) and more detailed RFI studies will follow in the next months.

Figure 1: Aerial view of the SRT site looking SE to NW.

4 Aperture array configurations

We intend to study the performances in terms of uv-coverage and angular resolution of an aperture array composed of a large number of small, fixed antenna elements plus receiver chains which can be arranged on the ground to form one or more stations. In particular, here we focus on an aperture array of a *fixed number of 128 antennas*. The definitive number of antennas is still to be decided and it will be a result of the compromise between the fraction of project budget required for the back-end and that needed for the array installation.

Considering the space available at the SRT site, we propose an aperture array composed by a core plus a few more distant satellite regions. The core is thought as a circular area of D=64 m in diameter while the satellite regions are four smaller circular region of D=15 m. The suggested locations for the 64 m core and the four 15 m satellite regions are shown in Fig. 2. The core region can be used either to deploy the antennas over a large region or to host 4 core stations of D=15 m (these are labeled C1, C2, C3, and C4 in Fig. 2).

This choice allow the implementation of different configurations for the aperture array, among which we consider the following possibilities:

i) all the antenna elements are clustered in the core to realize a single big station of 64 m in diameter (1-BIG configuration);

ii) the core and the satellite areas are used to form an aperture array composed by 4 small stations (e.g. S1,C1,C3, and S4) of 15 m in diameter. We call this the 4-SMALL configuration;

iii) the core and the satellite areas are used to form an aperture array composed by 8 small stations of 15 m in diameter. We call this the 8-SMALL configuration.

The approximated locations of the core and satellite stations are listed in Tab. 1
In the following we study the performance of these three configurations in terms of uv-coverage and angular resolution.

4.1 Station layout

There are two basic layouts that are generally considered for the distribution of the antennas in the stations of an aperture array:

i) a *dense* distribution having elements regularly spaced by $\leq \lambda/2$. As the frequency reduces, the arrays over-samples the incoming wavefront and the $A_{\rm eff}$ remains roughly constant. The advantage of a dense distribution is that the beam of the station is very well controlled leading to a high-dynamic range capability;

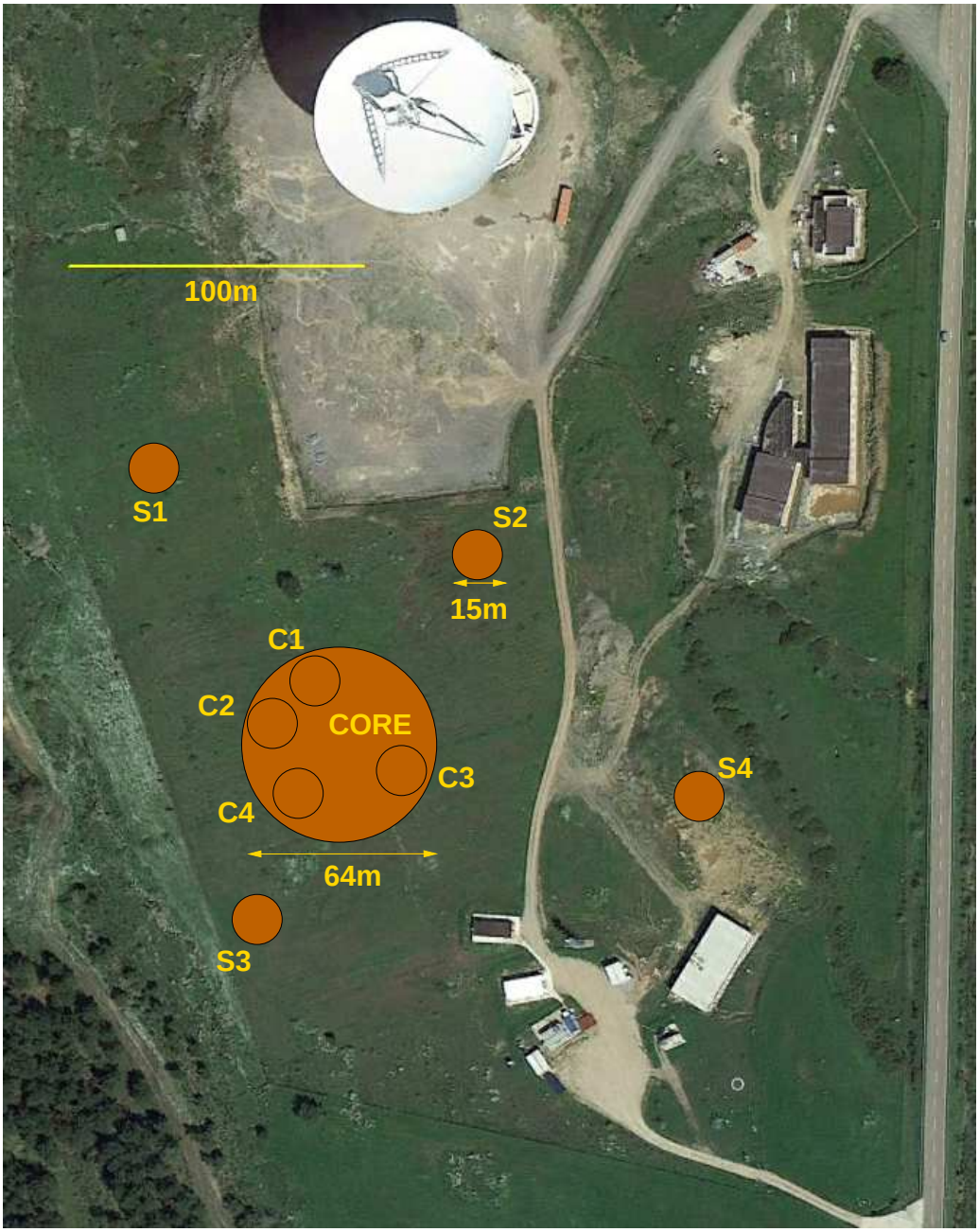

Figure 2: Suggested locations for the 64 m core and the four 15 m satellite regions.

Table 1: Approximate positions for the centers of the core and the satellite regions

Region	Latitude Degrees	Longitude Degrees	Height meters
Core	39.491181	9.244629	595
C1	39.491375	9.244534	593
C2	39.491244	9.244371	593
C3	39.491108	9.244876	596
C4	39.491046	9.244480	595
S1	39.492003	9.243916	589
S2	39.491745	9.245150	593
S3	39.490673	9.244325	597
S4	39.491045	9.245997	600

Table 2: Assumed fractional antenna efficiency η and $T_{\rm sys}$ as a function of elevation at $\nu = 327$ MHz. At El=90$^{\rm o}$ we assume $A_{\rm eff}/T_{sys} = 2.3 \times 10^{-3}$ m^2/K (1 polarization).

Elevation Degrees	η	$T_{\rm sys}$ K
0	0.0	95
30	0.41	95
45	0.67	95
60	0.87	95
75	0.97	95
90	1.00	95

ii) a *sparse* distribution with elements randomly spaced further apart than $\lambda/2$. If each antenna element samples the incoming wavefront independently the $A_{\rm eff}$ scales as λ^2. This behavior is particularly useful below $\sim$ 500 MHz where the sky is the dominant noise source, $T_{\rm sky} = 60 \times [\lambda/{\rm m}]^{2.6}$ K. The improvement in sensitivity is paid with a high level of beam side-lobes.

Indeed, at low frequencies sparse aperture arrays represent the preferred solution. However, it is mandatory to assess precisely the behavior of the beam at large distances from the pointing center since it impacts directly on the scientific performances of the array. For the purpose of the present study it is important to calculate some reasonable values for the $A_{\rm eff}$ and field-of-view (FoV) of the array stations and to predict, at least at a zero-order level, which is the beam shape resulting from different array configurations. The detailed design of each station, in terms of the number and the disposition of antennas, as well as the design of the single antenna itself, will be the subject of considerable study and simulation during the next stages of the SAD project. For now, we tentatively assume that each station will be constituted by antennas[2] characterized by $A_{\rm eff}/T_{sys} = 2.3 \times 10^{-3}$ m^2/K at $\nu = 327$ MHz and elevation El=90$^{\rm o}$. Furthermore, we assume that the fractional antenna efficiency scales as a function of elevation as listed in Tab. 2.

5 Beam-forming simulations

We simulate the beam-forming for both the 64 m and the 15 m stations. In this set of simulations we will show the beam pattern of the stations when the signal from the individual antennas are added coherently to reinforce the array response toward a given direction.

A simulation for configuration 1-BIG is shown in Fig. 3. In the left panel we show the aperture array of this single station where all the 128 antennas are randomly sparse to within the core region. The average spacing between the antennas is of about 3.5 m. This implies that the station is a sparse array in all the considered frequency range of 70 - 450 MHz (i.e. wavelength ranging from 4.3 to 0.66 m). Indeed, we simulated the expected beam of station by supposing that the antenna elements are acting independently one from each other. We calculate the response in elevation of each antenna by interpolating the values in Tab. 2. We calculated the expected geometry delays on each antenna element as a function of azimuth and elevation with respect to the geometrical center of the station by supposing that the array is planar. By compensating for these delays we are able to form the beam at any given direction in the sky. In Fig. 3 we show the results of our simulation for $\nu = 327$ MHz. In the top middle-panel we show the all sky image (in orthographic projection; SIN) for the beam-forming at the zenith. In the bottom middle-panel we show a zoom of the beam over a Fov of 5$^{\rm o}\times$ 5$^{\rm o}$. The beam is circular with a FWHM of about 1.16$^{\rm o}$. We note that, differently from a single-dish beam that decreases rapidly away from the pointing center, the sparse array beam at large angular distance from the peak does not falls off to zero but rather oscillates around a plateau of about 0.7% the peak (-21.5 dB) with a rms scatter of 5% (-13 dB). The right-panels illustrates the beam forming at El=45$^{\rm o}$ and Az=180$^{\rm o}$. The all-sky image in the top-right panel shows the decrease of the antennas $A_{\rm eff}$ at elevations below El<30$^{\rm o}$. The bottom-right panel shows a zoom of the beam which is elliptical with FWHM of 1.72$^{\rm o}\times$1.16$^{\rm o}$ and PA 0$^{\rm o}$.

We then repeated the simulations for satellite stations of D=15 m. We considered two random arrays of 32 and 16 antennas and for comparison we consider also one tile array of 4×4 antennas. For all the three, the average distance between the antennas is about 2-3 meters so that they can all be considered sparse arrays too. The beam-forming simulations are show in Fig. 4. The beam FWHM for both the two random arrays of 32 and 16 antennas is of about 5$^{\rm o}$ since the antennas are spread over the same region, but obviously the 32 antennas station has a lower side lobes level. The compact tile array has regular pattern but the few secondary positive and negative side lobes are very high compared to a random array with the same number of antennas.

We summarize the results of the beam-forming simulations in Tab. 3.

[2]These are roughly the expected numbers for a Vivaldi antenna element of about 1 meter in size.

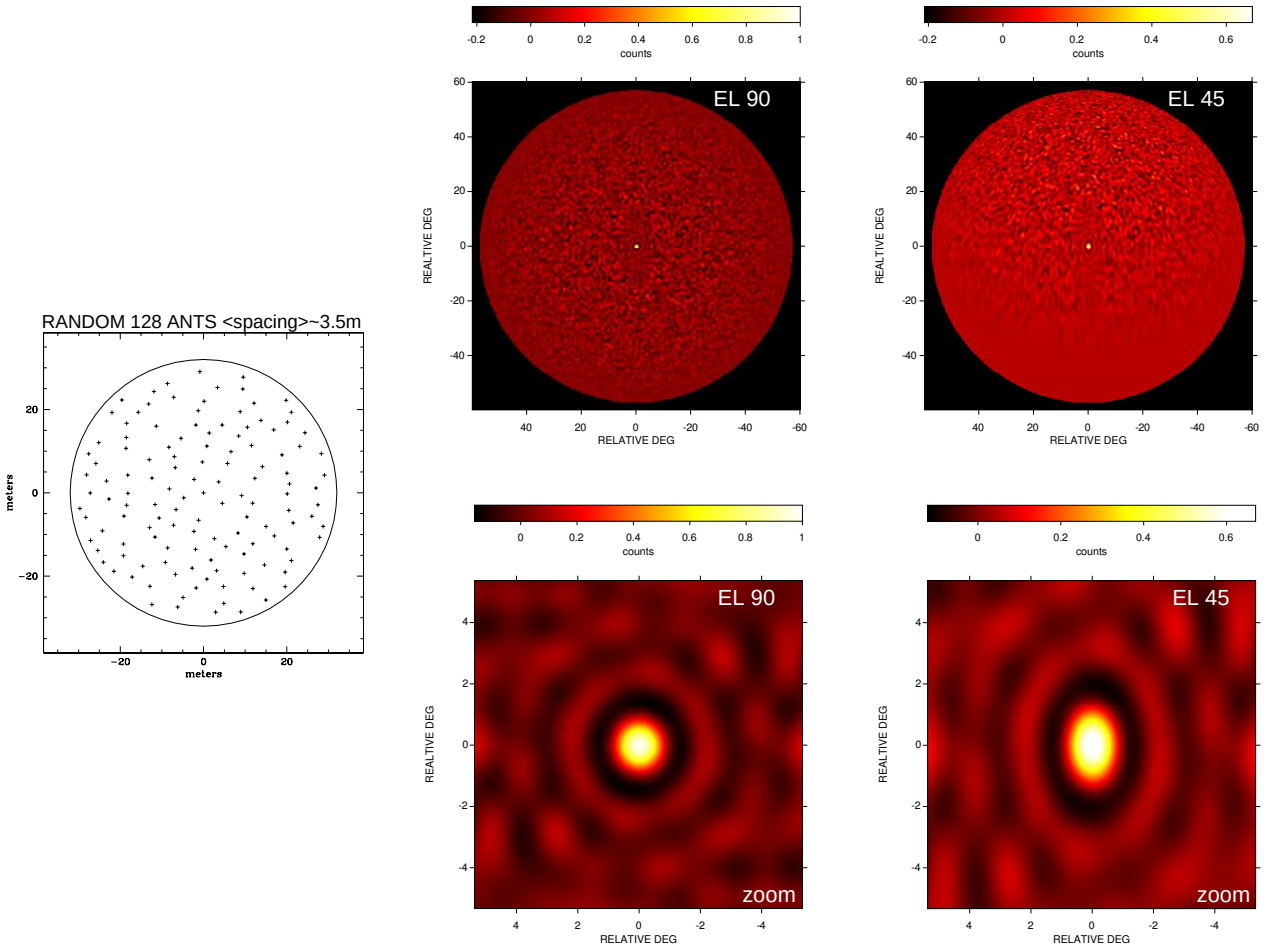

Figure 3: Beam-forming simulation for 1-BIG station (SIN projection).

Table 3: Beam forming simulations for a pointing at the zenith (El=90°) and ν = 327 MHz.

Station	N antennas	D meters	⟨spacing⟩ meters	FWHM beam degrees	average side lobe level	rms side lobe level
BIG	128	64	3.5	1.16	0.7%	5%
SMALL	32	15	2	4.8	2%	10%
SMALL	16	15	3	4.8	6%	15%
TILE	16	6	2	8	–	–

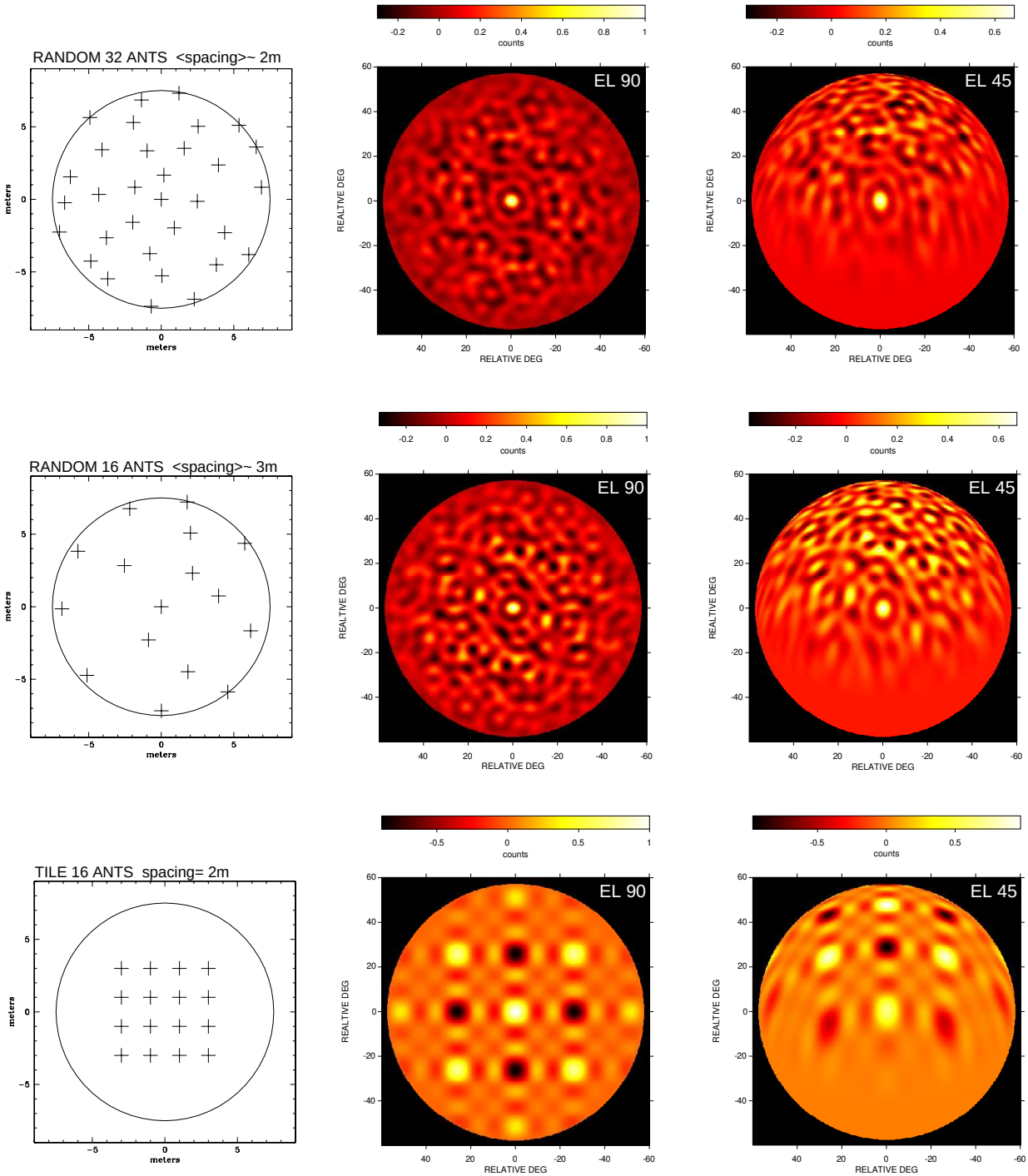

Figure 4: Beam-forming simulations for small stations (SIN projection).

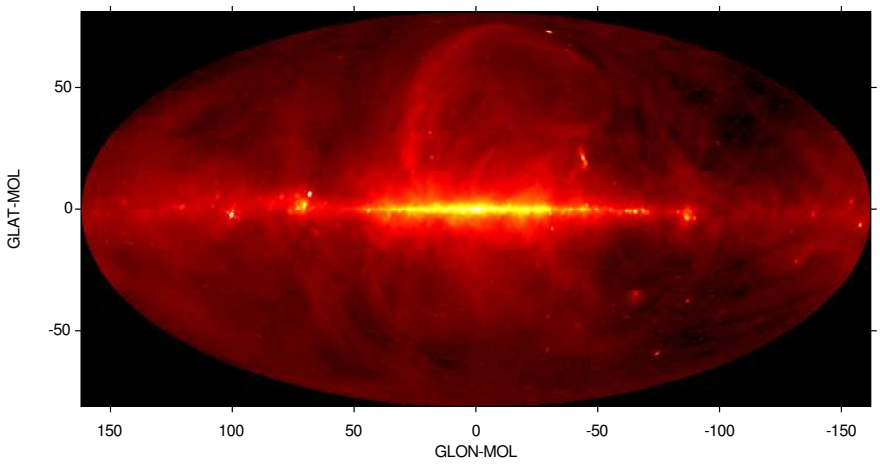

Figure 5: All-sky model at $\nu = 327$ MHz used for the 1-BIG configuration (Mollweide projection).

6 Interferometric simulations

We perform a set of simulations in which the signals from the single antennas or stations are correlated to produce an interferometric image of the sky. In this way, we are able to estimate, at zero order level, the imaging capabilities of the different configurations of the aperture array (1-BIG, 4-SMALL, and 8-SMALL) in terms of uv-coverage, angular resolution, sensitivity, and dynamical range.

Our intent is to reproduce an hypothetical interferometric observation conducted in the frequency range of interest 70 - 450 MHz. For simplicity, we considered an observation conducted at 327 MHz (i.e. $\lambda \simeq 0.92$ m) with a narrow bandwidth of 16 MHz.

6.1 1-BIG

The 1-BIG aperture array can be used as a phased station using beam-forming (see Sect. 5). Another possibility is to use the N=128 antennas of the aperture array as if they were elements of an interferometer with $N \times (N-1)/2 = 8128$ baselines.

In beam-forming mode only one-region of the sky can be pointed at a time. Thus, the simultaneous observations of different pointings requires to apply a specific set of beam-forming coefficients for each direction. The situation is radically different in interferometric mode where the FoV is very large being essentially the wide beam of the single antennas ($\simeq 60^{\rm o}$). Indeed, by correlating, rather then by summing, the signals from the antennas we can in principle obtain from a single integration time an image of the entire sky.

To test this possibility, we first obtained a model of all-sky emission at 327 MHz by rescaling the data from the Haslam 408 MHz radio continuum sky survey (Haslam et al. 1982) with a spectral index $\alpha = 0.8$, which should be appropriated for the galactic foreground and most extragalactic point sources. The original resolution of the survey FHWM $0.8^{\rm o}$ is only slightly smaller than the expected beam of the 1-BIG antenna but still useful for our purposes. The all-sky model, in galactic coordinates, is presented in Fig.5.

We simulate how the all-sky emission would be seen in a single snap-shot of 10 seconds obtained by the 1-BIG antenna with a bandwidth of 16 MHz centered at 327 MHz. We focus on a simulation with the phase center at the zenith, so that the 1-BIG aperture array can be considered planar. The uv-coverage is shown in the top-middle panel of Fig. 6. The corresponding synthesized beam is circular with FWHM of $0.84^{\rm o}$ which is smaller than the beam-forming FWHM of $1.16^{\rm o}$ (see Sect.5). We reprojected the sky model to simulate the sky seen at the SRT site at LST 17:45, so that the Galactic Center is culminating.

We then obtained the simulated visibility data by convolving the sky model with the primary beam response of the single antennas and we add to the complex visibilities data a Gaussian random noise by assuming the $A_{\rm eff}$, $T_{\rm sys}$, and η reported in Tab. 2. The amplitude of the visibility as a function of the uv-distance is plotted in the middle-bottom panel of Fig. 6 while the corresponding deconvolved image is shown in the bottom-right panel. We find a rms noise of 45 Jy/beam. This is much higher than the expected thermal noise which can estimated by the equation

$$\sigma_{\rm thermal} = \frac{SEFD}{\eta_c \sqrt{n_{\rm pol} N(N-1)\Delta\nu\, t_{\rm int}}} \quad ({\rm Jy/beam}) \tag{1}$$

here the factor η_c encodes the "back-end" efficiency which accounts for all losses due to the digital processing and

does not include the antenna efficiency. This loss factor depends on several effects like effective integration time resulting from transmission dead times or the quantizer losses. These performances are still unknown for the SAD back-end and we assume $\eta_c = 0.8$. The "system equivalent flux density", defined $SEFD = 2k_B T_{\rm sys}/A_{\rm eff}$, takes into account of the efficiency and the collecting area of the single antenna element, plus the system noise. In our case at the zenith SEFD=1.2 MJy and hence for $t_{\rm int} = 10$ sec, $\Delta\nu = 16$ MHz, and $n_{\rm pol}$=2 we expect $\sigma_{\rm thermal} \simeq 0.6$ Jy/beam.

Note that the theoretical rms noise calculated using equation 1 is the best limit possible. There are other factors that will tend to increase the noise compared with theoretical. One of the most relevant at low frequencies is the confusion noise resulting from faint radio sources blended within the synthesized beam:

$$\sigma_{\rm confusion} = 0.2 \left(\frac{\nu}{\rm GHz}\right)^{-0.7} \left(\frac{\theta_{\rm b}}{\rm arcmin}\right)^{2} \quad ({\rm mJy/beam}) \tag{2}$$

see Condon (2002). Given the synthetized beam of the 1-BIG antenna we expect a confusion noise at 327 MHz of $\sigma_{\rm confusion} = 1.2$ Jy/beam. By adding in quadrature the thermal noise and the confusion noise we would expect rms noise fluctuations of a few Jy/beam, i.e. much lower than what obtained in the simulated image. However, we must consider an additional type of confusion which generally affects low frequency observations: the confusion from the side lobes of uncleaned sources lying within the primary beam and often from strong sources in the side lobes of the primary beam. This is by far the most relevant noise in our case since the primary beam is extremely wide and the side lobe level very high (see Sect. 5). Indeed, the sensitivity is expected to be largely limited by the dynamical range and a deep clean is required. However, due to practical computational issues[3] we just performed a very shallow deconvolution of the dirty beam for the image presented in the bottom panel of Fig. 6. Nevertheless, for the illustrative purpose of this document, this is enough to show that with just 10 seconds of integration time we have sufficient sensitivity to detect not only the most bright point sources in the sky (Cas-A, Cyg-A, and Vir-A) but also extended features such as the galactic plane and the Cygnus-X star-forming complex.

We note that the resolution of the synthesized beam is slightly finer than that obtained through beam-forming. This non trivial result could arise from the different weighting schemes adopted in the two approaches and further investigation is needed to understand this behavior. Moreover, also the side lobes level of the synthesized beam is much better. In fact, the average plateau level is zero while the rms is just about 0.8%, *i.e. one order of magnitude less than the side lobes rms obtained through beam forming*, see Fig. 7. This effect could be due to the radically different method used combine the signals from the antennas (multiplicative instead of additive correlation).

6.2 4-SMALL and 8-SMALL

In these simulations we assumed that the aperture array is configured in a set of 4 or 8 stations of D=15 m. Beam-forming is performed at station level to form a small number of relatively long baselines (a hundreds of meters in our case) between the phased array stations thus improving significantly the angular resolution of the aperture array by using the so-called Earth rotation synthesis technique.

The simulations have been performed with the NRAO software package AIPS. Starting from a realistic sky model, we generated the corresponding u-v data for the aperture array in the 4-SMALL and 8-SMALL configurations. The antenna $A_{\rm eff}$ and $T_{\rm sys}$ are used to calculate the Gaussian noise appropriate for each visibility. For the 4-SMALL configuration we assume to have 4 stations with 32 antennas each, while for the 8-SMALL configuration we assume 8 station with 16 antennas each. Following the result obtained in Sec. 5, the primary beam of the stations is taken ~5° at the zenith for both configurations.

However, we note that the primary beam of the stations is variable. The projection of the antenna station aperture on the source picture plane is changed depending on the source elevation. The beam of the antenna station is approximated to be circular two dimensional Gaussian at zenith with FWHM 5°, while it is considered elliptical two dimensional Gaussian with the major axis increased by a factor of 1/sin(El) as the elevation changes. In practice, at each time the Gaussian beam is rotated to direct the BMAJ in the calculated azimuth while BMIN stays constant to 5°.

We extracted a sky model from the Westerbork Northern Sky Survey (WENSS, Rengelink et al. 1997) which was performed at 325 MHz. The sky model is obtained from a field of view of more than about 15°×15° around the bright radio source 3C84 at the center of the Perseus galaxy cluster: RA $3^h\ 19^m\ 47^s$ and DEC $41^d\ 30^m\ 43^s$ (J2000). A zoomed image of the sky model is shown in Fig. 8. This field has been selected because of the presence of the very well-known bright source 3C84 (18 Jy at 327 MHz) and for the presence of other extended radio sources of lower flux densities which make it an ideal field to test the dynamical range capabilities of the array. Starting from this sky model we produce the visibility data as would be obtained by the array in the two configurations.

Here, we look for the configuration that provides the most promising performances in terms of uv-coverage and angular resolution. Indeed, good uv-coverage and resolution are necessary for a scientific validation of the array based on the observation of astronomical radio sources. We note, however, that the proposed configurations may yet require slightly different installation efforts in terms of terrain preparation, optical fiber deployment, and so on. Although these

[3] Although the array is planar as seen from the zenith, the FoV is so large that its curvature requires a 3D deconvolution anyway.

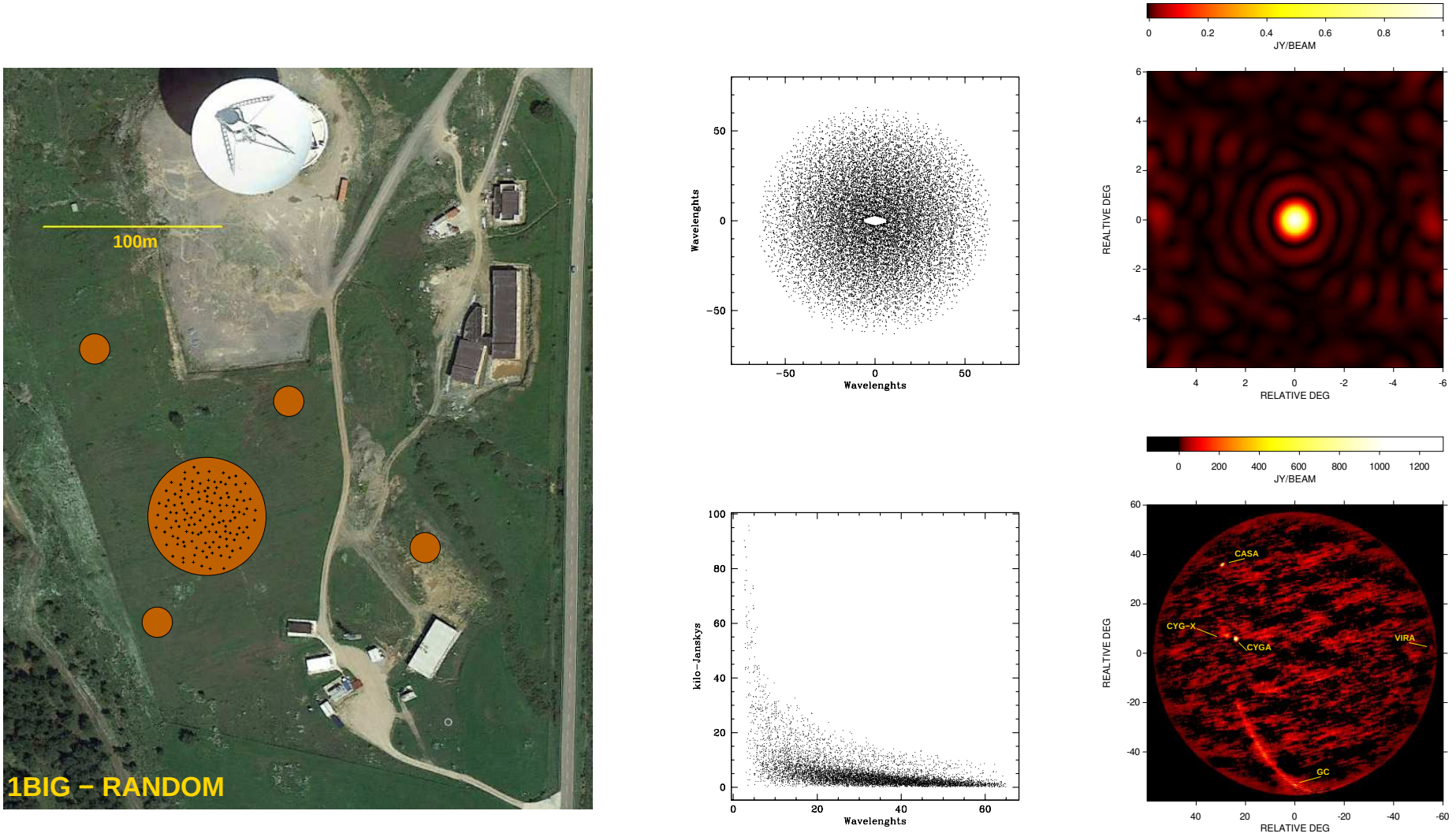

Figure 6: Array configuration 1-BIG. Simulation results for a **10 seconds snap-shot observation** with 16 MHz bandwidth at a central frequency of 327 MHz (0.92 m wavelength). *Middle-top:* uv-coverage. *Top-right:* synthesized beam. The FWHM is 0.84°× 0.84° with PA=0°. *Middle-bottom:* visibility amplitude versus the uv-distance. *Bottom-right:* Partially CLEANed image showing a zenithal view of the sky in SIN projection. The noise level is of $\sigma \simeq 45$ Jy/beam. The estimated confusion noise is of 1.2 Jy/beam while the expected thermal noise level is about 0.6 Jy/beam.

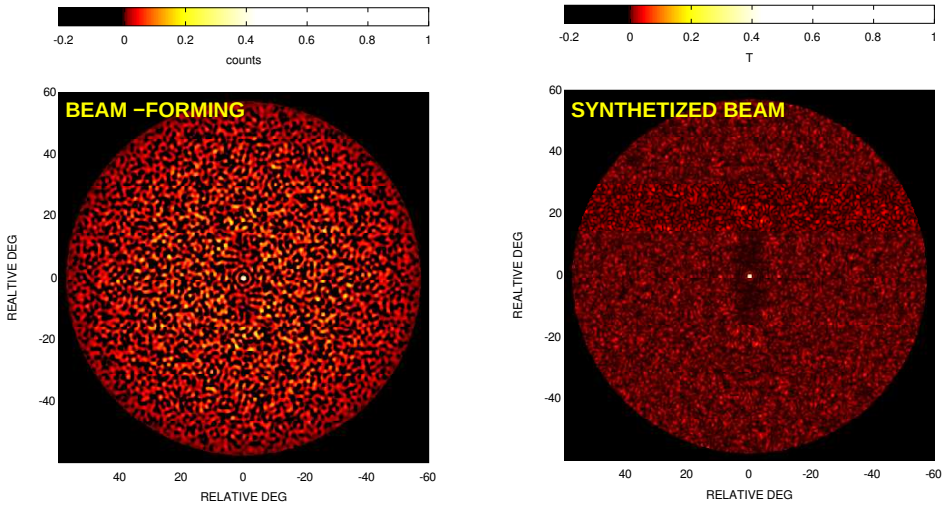

Figure 7: Beam-forming (left) vs synthesized beam (right) for 1-BIG configuration shown in the same scale and field of view. The image shown in the left-panel is the same as that in Fig.3 middle-top panel but here shown with a different color range saturation. The image shown in the right panel is the same as that in Fig.6 top-right panel but here shown for a larger field of view.

issues are not directly addressed by the present document, they definitely play a crucial role in determining which is the most suitable configuration for the SAD.

The 4-SMALL configuration has baselines which span a range of 40 to 250 wavelengths for C1-C3 and S1-S4, respectively. The 8-SMALL configuration has 28 baselines in the range from 20 to 250 wavelengths (C1-C2 and S1-S4), respectively.

Simulation results are presented in Figures 9 to 12. On top-middle panels, we present the coverage of the u-v plane where we average the tracks of different frequency channels within the 16 MHz bandwidth. Middle-bottom panels show the amplitude of the visibility fringes versus the uv-distance obtained by averaging over all frequency channels. The synthesized beam is shown in the top-right panels while in the bottom-right panels we present the CLEANed image corresponding to the same FoV showed in Fig. 8.

For both configurations we imposed an elevation limit of 25^{o} and we produced a full-synthesis 12 h observation and a 'snap-shot' 1 h observation.

6.2.1 Full-synthesis simulation results

Full-synthesis simulation results are shown in Fig. 9 and 10. The simulated synthesized beam is from $16' \times 10'$ for 4-SMALL and $15' \times 13'$ for 8-SMALL, respectively. For both configurations the final noise level is still higher than the thermal noise but somewhat lower than the expected confusion limit from Eq. 2. This bias is likely due to the flux density limit imposed in selecting the components from the WENSS model. By cutting out the fainter radio sources, we artificially reduced the confusion noise.

The uv-coverage and hence the dynamical range is clearly better for the 8-SMALL. The uv-coverage for the 4-SMALL is poorer but the resolution is higher because long baselines have a higher weight over the short ones. Indeed, although the dynamical range is worse the comparatively higher resolution provides a lower confusion limit if compared with the 8-SMALL. In conclusion, as far as a full-synthesis is considered, the 4-SMALL and the 8-SMALL provide similar imaging performances.

6.2.2 Snap-shot simulation results

Snap-shot simulation results are shown in Fig. 11 and 12. The 4-SMALL and 8-SMALL configurations have very different performances for snap-shot observation. The 4-SMALL stations are aligned NW-SE, resulting in very poor and elongated beam. Imaging is prohibitive in these conditions. On the other hand, the 8-SMALL still gives a reasonable sampling of the uv-plane and hence a minimum imaging capability is possible.

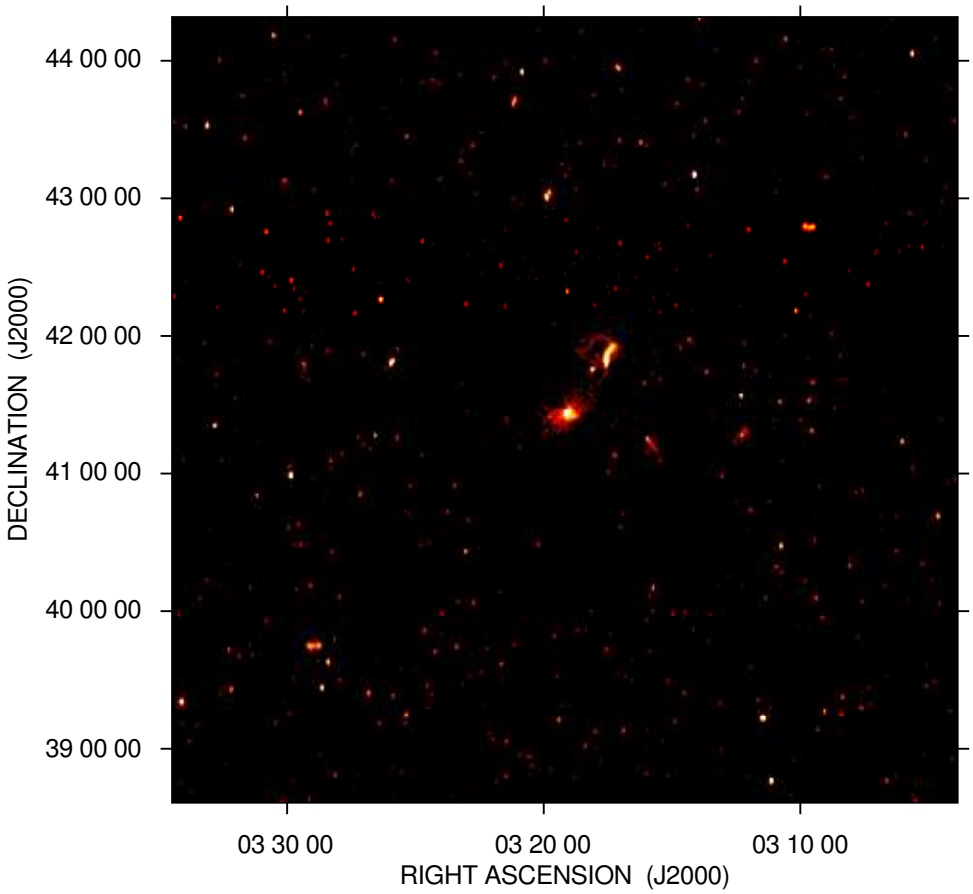

Figure 8: Inner portion of the sky model showing a FoV of 5°×5° around the bright radio source 3C84 at the center of the Perseus galaxy cluster. The whole sky model spans a FoV of 15°×15°.

7 Concluding remarks

7.1 Caveat of the simulations

In evaluating the results presented here, it should be considered that the simulations we performed are based on several approximations and many relevant effects have not been included. Among the most important:

i) we lack of a real characterization of the station parameters like primary beam, A_{eff}, T_{sys};

ii) the station primary beam for 4-SMALL and 8-SMALL simulations is considered Gaussian but in the real case significant side-lobes are expected;

iii) the bandpass response function of the antennas has been neglected;

iv) the tropospheric and ionospheric distortions on the visibility data are not included;

v) the effects of the RFI contamination are ignored;

vi) the confusion noise is only partially included since we imposed a flux limit cut to the sky model;

vii) all complications related to wide-band calibration of large FoV at low-frequencies have not been addressed.

Moreover, an accurate simulation of the effective noise level expected in these observations will be possible only when the antenna efficiencies and system temperature will be known with sufficient precision.

We note, however, that for the 1-BIG configuration in snap-shot mode the noise is limited by dynamical range. Thus, the sensitivity can be improved by a sky-model subtraction and/or a deep deconvolution of the dirty beam.

For the full-synthesis observations with 4-SMALL and 8-SMALL configuration the final noise is limited by confusion. In both cases the thermal noise is expected to be much lower. Thus to improve the sensitivity of 4-SMALL and 8-SMALL the only possibility is to improve the resolution of the aperture array by adding stations with baselines much longer than 200 m.

7.2 Best compromise for the array configuration

To summarize, on the basis of the results reached in this report, we propose for SAD one core region of 64 m in diameter plus four satellite stations of 15 m in diameter. The core region may host up to four additional stations of 15 m in diameter, eventually. Indeed, this disposition for the aperture array offers the possibility to modulate the development of the project in steps of increasing complexity without precluding any configuration (or re-configuration) a priori.

For example, it will be possible to concentrate all the antennas in the core, that perhaps represents a easier installation. With the 1-BIG configuration we could start with the first beam-forming tests. Moreover, simulations showed the 1-BIG aperture array can be also employed as an interferometer to realize all sky images at a resolution of about 0.8^{o}, realizing a sort of real-time 'radio planetarium'. This technique has been already implemented with the first Long Wavelength Array antenna (see http://www.phys.unm.edu/ lwa/lwatv.html) at frequencies below 80 MHz. With the 1-BIG station we will be able to extend this real-time monitoring to the complementary frequency range 70-450 MHz at the SRT site.

On the other hand, it will also possible to deploy the antennas in up to 8 different smaller stations of D=15 m, realizing an aperture synthesis array with a maximum baseline of about 200 m, thus combining beam forming at a station level and interferometry between stations. The simulations presented in this study show that confusion limited images could be possible at resolution of about $15'$ and FoV of about 5^{o}.

In conclusion, an aperture array configurable on a core of 64m in diameter plus four small station of 15m will provide the necessary sensitivity and angular resolution to perform useful scientific tests and at the same time it will guarantee modularity and scalability of the project.

7.3 Other developments

The SAD represents an European bench test to verify on the field the new technologies developed to observe the low frequency radio sky. The basic configuration of SAD will permit to perform basic scientific experiments but with additional resources it would be possible to expand the capabilities of the array enabling more advanced tests. In particular, by observing in combination with the SRT it will be possible to test innovative beam forming techniques which could be potentially of interest for the SKA.

8 References

Calabretta & Greisen, A&A 395, 1077, 2002

Condon 2002, ASP Conf. 278, 155

F. Govoni, P. Bolli, F. Gaudiomonte, M. Murgia, R. Ambrosini, C. Bortolotti, J. Monari, F. Perini, M. Roma - "Low-frequency RFI investigation at the SRT site", OA-Cagliari Internal Report N. 24, 2013

Haslam, Stoffel, Salter & Wilson 1982 A&AS, 47, 1

M. Murgia, F. Gaudiomonte, G.Serra, F. Govoni, J. Monari, F. Perini, M. Schiaffino, P. Bolli - "Low-frequency RFI measurements at the SRT site performed with the Vivaldi v2.0 antenna", OA-Cagliari Internal Report N. 31, 2013

Synthesis Imaging in Radio Astronomy II, Edited by G.B Taylor, C.L. Carilli, and R.A Perley, ASP Conference Series Voume 180.

Rengelink et al 1997, A&A Suppl. 124, 259.

9 Acknowledgments

We thank Joseph Lazio for useful discussions and suggestions. Satellite images of the SRT site have been taken from Google Earth. AIPS is produced and maintained by the National Radio Astronomy Observatory, a facility of the National Science Foundation operated under cooperative agreement by Associated Universities, Inc.

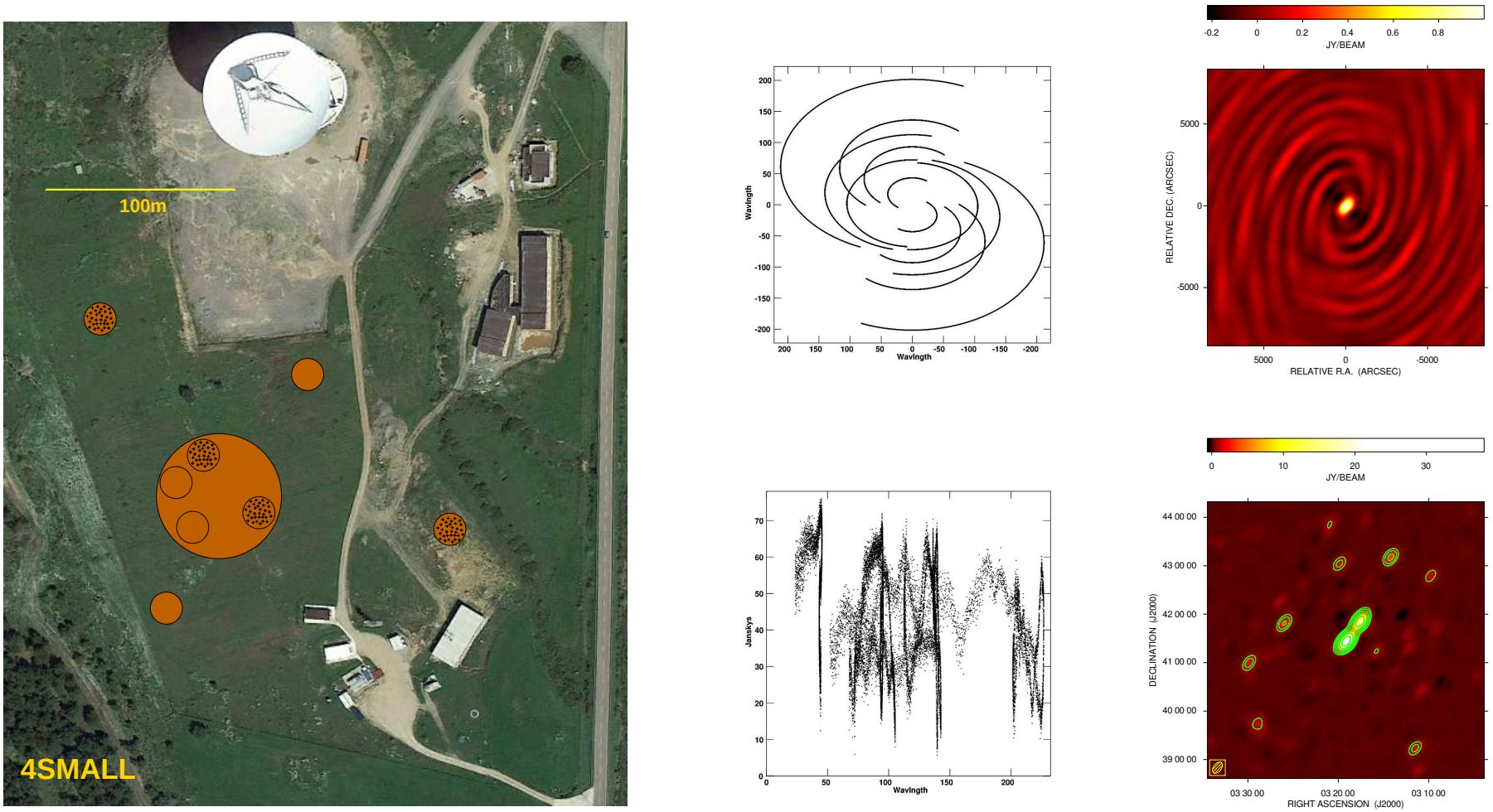

Figure 9: Array configuration 4-SMALL. Simulation results for a **full-synthesis 12 hours observation** with 16 MHz bandwidth at a central frequency of 327 MHz (0.92 m wavelength). *Middle-top:* uv-coverage. *Top-right:* synthesized beam. The FWHM is 16.1′× 9.7′ with PA=-37.1°. *Middle-bottom:* visibility amplitude versus the uv-distance. *Bottom-right:* CLEANed image showing a field of view of about 5°×5° around 3C 84. The noise level is of $\sigma \simeq 24$ mJy/beam. Contour levels start at 3σ and increase by a factor of 2. The estimated confusion noise is of 68 mJy/beam while the expected thermal noise level is about 17 mJy/beam.

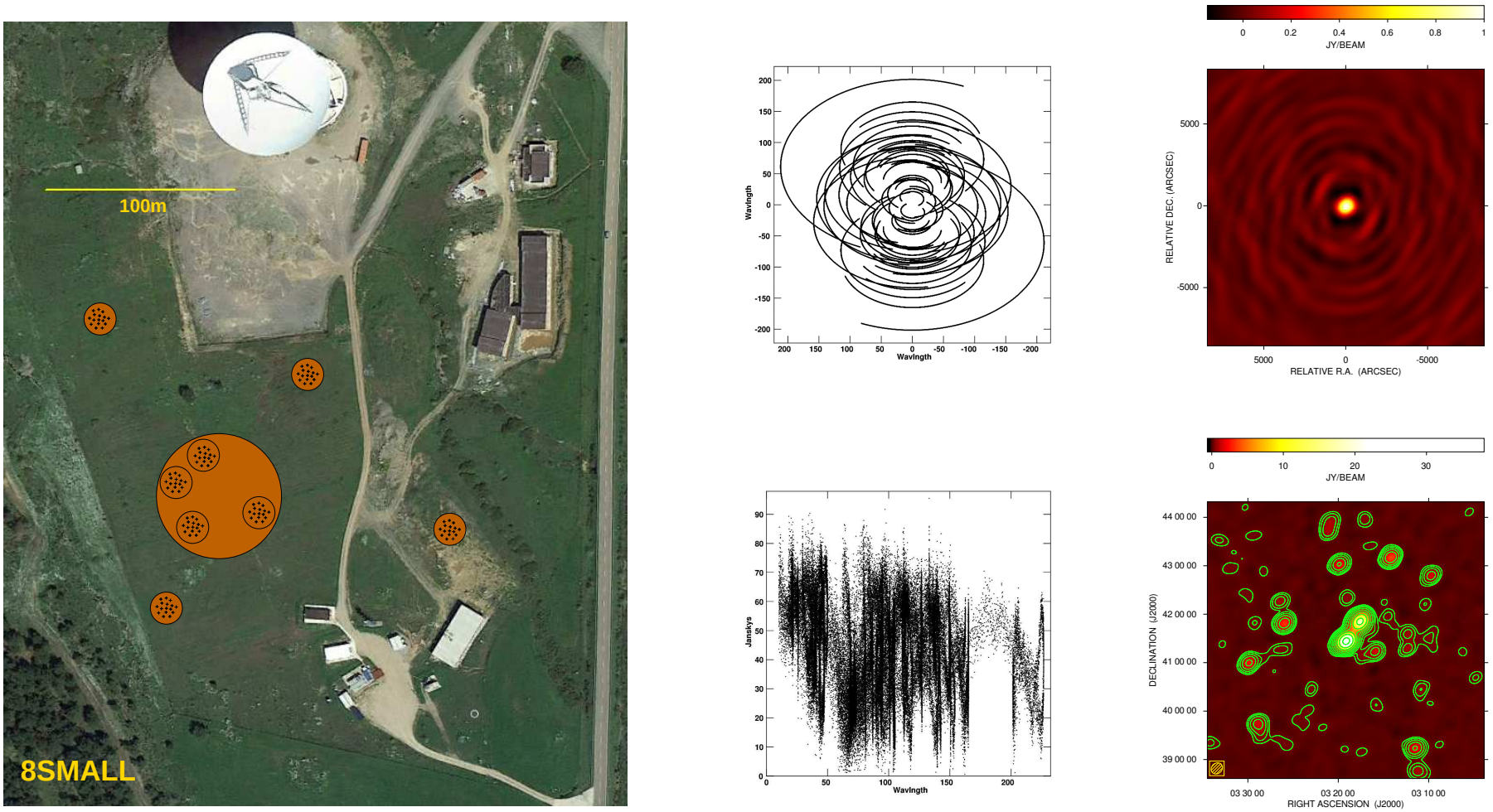

Figure 10: Array configuration 8-SMALL. Simulation results for a **full-synthesis 12 hours observation** with 16 MHz bandwidth at a central frequency of 327 MHz (0.92 m wavelength). *Middle-top:* uv-coverage. *Top-right:* synthesized beam. The FWHM is 15.0′× 12.8′ with PA=-48.30°. *Middle-bottom:* visibility amplitude versus the uv-distance. *Bottom-right:* CLEANed image showing a field of view of about 5°×5° around 3C 84. The noise level is of $\sigma \simeq 37$ mJy/beam. Contour levels start at 3σ and increase by a factor of 2. The estimated confusion noise is of 84 mJy/beam while the expected thermal noise level is about 16 mJy/beam.

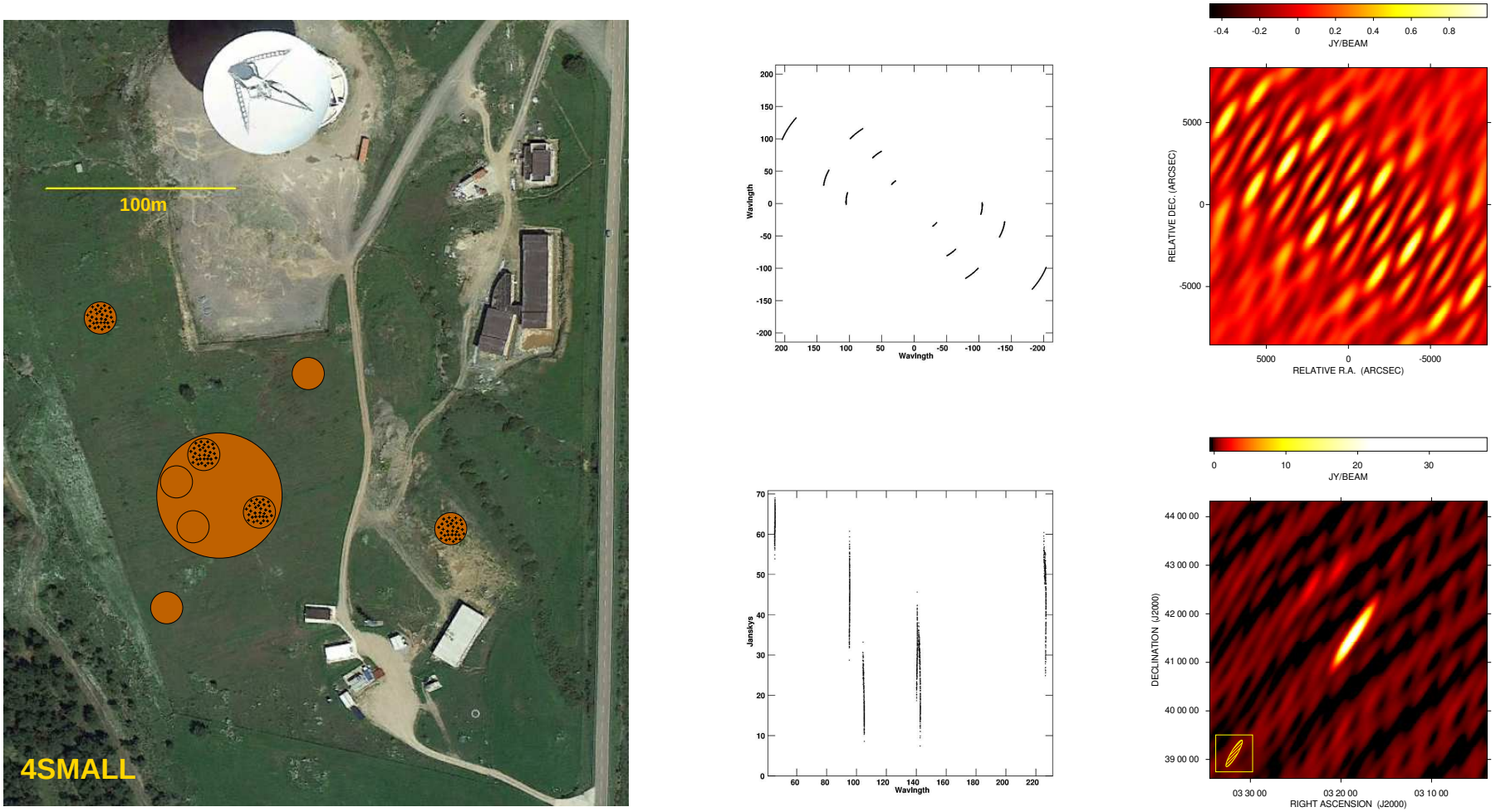

Figure 11: Array configuration 4-SMALL. Simulation results for a **snapshot 1 hour observation** with 16 MHz bandwidth at a central frequency of 327 MHz (0.92 m wavelength). *Middle-top:* uv-coverage. *Top-right:* synthesized beam. The FWHM is 103′× 5.8′ with PA=-45.8°. *Middle-bottom:* visibility amplitude versus the uv-distance. *Bottom-right:* CLEANed image showing a field of view of about 5°×5° around 3C 84. The noise level is of $\sigma \simeq 340$ mJy/beam. Contour levels start at 3σ and increase by a factor of 2. The estimated confusion noise is of 261 mJy/beam while the expected thermal noise level is about 58 mJy/beam.

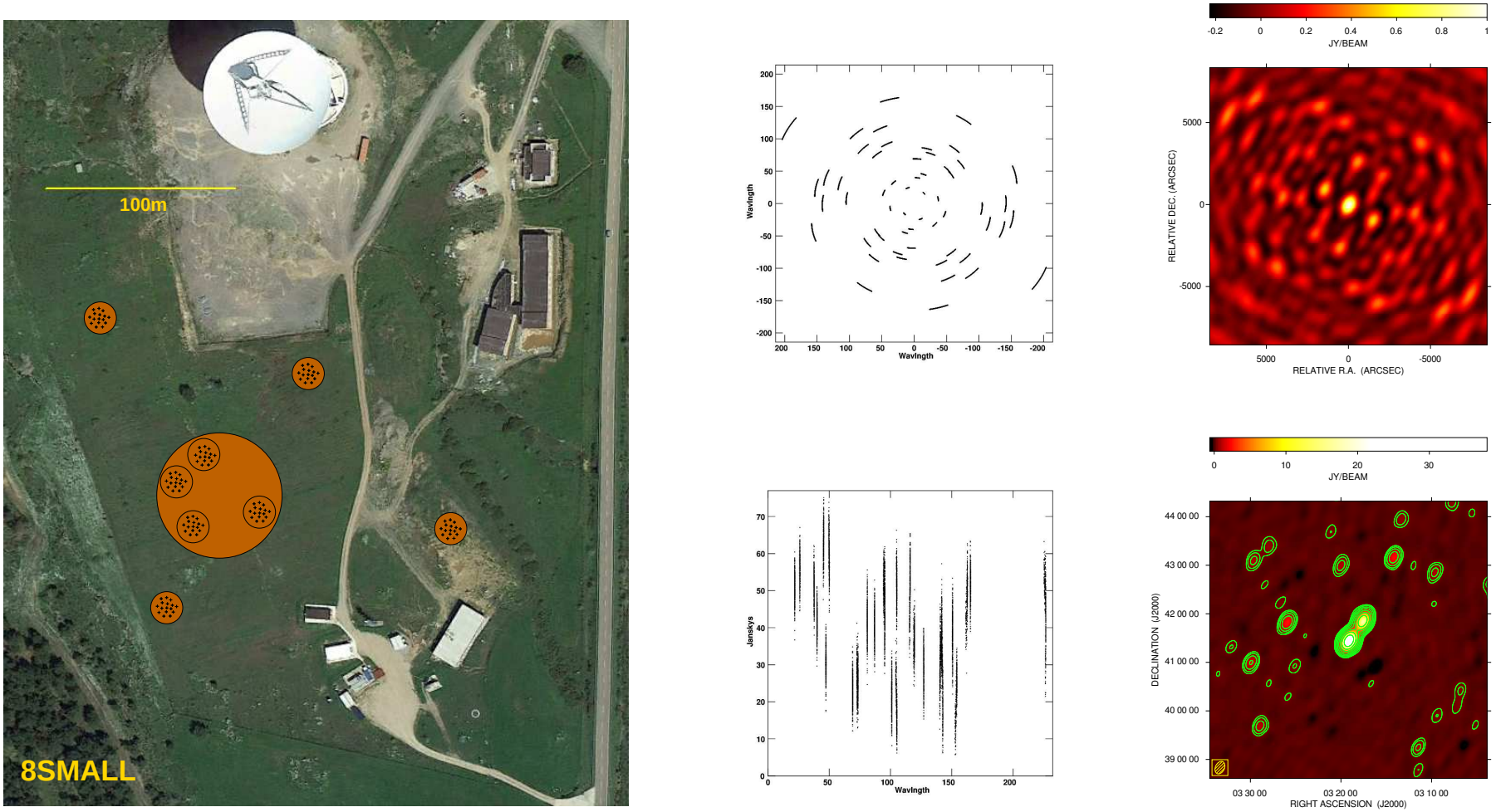

Figure 12: Array configuration 8-SMALL. Simulation results for a **snapshot 1 hour observation** with 16 MHz bandwidth at a central frequency of 327 MHz (0.92 m wavelength). *Middle-top:* uv-coverage. *Top-right:* synthesized beam. The FWHM is 16.3′× 11.2′ with PA=-25.95°. *Middle-bottom:* visibility amplitude versus the uv-distance. *Bottom-right:* CLEANed image showing a field of view of about 5°×5° around 3C 84. The noise level is of $\sigma \simeq 54$ mJy/beam. Contour levels start at 3σ and increase by a factor of 2. The estimated confusion noise is of 80 mJy/beam while the expected thermal noise level is about 54 mJy/beam.